AD-A056 790 GRUMMAN AEROSPACE CORP BETHPAGE N Y RESEARCH DEPT F/G 20/4
COMPUTATIONS OF JET IMPINGEMENT ON A FLAT SURFACE,(U)
JAN 78 A RUBEL N00014-77-C-0524
UNCLASSIFIED RM-650J NL

1 OF 1
ADA
056790

END
DATE
FILMED
9 78
DDC

RM-650J

COMPUTATIONS OF JET IMPINGEMENT ON A FLAT SURFACE

June 1978

(12)

Grumman Research Department Memorandum RM-650J

COMPUTATIONS OF JET IMPINGEMENT ON A FLAT SURFACE*

by

Arthur Rubel

Aerophysics

June 1978

*Paper presented at the AIAA 16th Aerospace Sciences Meeting, Huntsville, Alabama, January 16-18, 1978

Approved by: Richard A. Scheuing
Director of Research

UNCLASSIFIED

SECURITY CLASSIFICATION OF THIS PAGE (When Data Entered)

REPORT DOCUMENTATION PAGE

READ INSTRUCTIONS BEFORE COMPLETING FORM

1. REPORT NUMBER

2. GOVT ACCESSION NO.

3. RECIPIENT'S CATALOG NUMBER

4. TITLE (and Subtitle)
(6) Computations of Jet Impingement on a Flat Surface

5. TYPE OF REPORT & PERIOD COVERED
78-207
Reprint of AIAA Paper

6. PERFORMING ORG. REPORT NUMBER

7. AUTHOR(s)
(10) Arthur Rubel

8. CONTRACT OR GRANT NUMBER(s)
(15) N000014-77-C-0524

9. PERFORMING ORGANIZATION NAME AND ADDRESS
Grumman Aerospace Corporation
Bethpage, New York 11714

10. PROGRAM ELEMENT, PROJECT, TASK AREA & WORK UNIT NUMBERS
NR 061-251

11. CONTROLLING OFFICE NAME AND ADDRESS
Office of Naval Research
Arlington, Virginia 22217

12. REPORT DATE
(11) January 1978

13. NUMBER OF PAGES

14. MONITORING AGENCY NAME & ADDRESS (if different from Controlling Office)
(12) 43 p.

15. SECURITY CLASS. (of this report)
Unclassified

15a. DECLASSIFICATION/DOWNGRADING SCHEDULE

16. DISTRIBUTION STATEMENT (of this Report)

This document has been approved for public release and sale; its distribution is unlimited.

17. DISTRIBUTION STATEMENT (of the abstract entered in Block 20, if different from Report)
(14) RM-6505

18. SUPPLEMENTARY NOTES

19. KEY WORDS (Continue on reverse side if necessary and identify by block number)

Jet Impingement

20. ABSTRACT (Continue on reverse side if necessary and identify by block number)

An incompressible, inviscid rotational flow model is used to represent the normal impingement of axisymmetric jets and the oblique impingement of two-dimensional jets upon a flat surface. The Poisson-type equation that results from this formulation is cast into suitable finite difference form and solved by relaxation techniques. Results, in terms of the ground plane pressure distribtuion, centerline velocity decay, and oblique impingement flow field structure, compare well with observations.

DD FORM 1 JAN 73 1473 EDITION OF 1 NOV 65 IS OBSOLETE
S/N 0102-014-6601

UNCLASSIFIED
SECURITY CLASSIFICATION OF THIS PAGE (When Data Entered)

406 165

COMPUTATIONS OF JET IMPINGEMENT ON A FLAT SURFACE†

A. Rubel*
Grumman Aerospace Corporation
Bethpage, New York 11714

Abstract

An incompressible, inviscid rotational flow model is used to represent the normal impingement of axisymmetric jets and the oblique impingement of two-dimensional jets upon a flat surface. The Poisson-type equation that results from this formulation is cast into suitable finite difference form and solved by relaxation techniques. Results, in terms of the ground plane pressure distribution, centerline velocity decay and oblique impingement flow field structure, compare well with observations.

Introduction

During lift-off of VTOL aircraft, turbulent lifting jets mix with the surroundings and impinge upon the ground, producing wall jets which interact to form upwash regions of high static pressure. These phenomena and their induced secondary flows produce lifting forces on the aircraft as well as suckdown and attendent lift losses. An understanding of the behavior of these complex flow fields is required for the optimization of VTOL design.

Efforts to analyze the overall nature of the interactions via the numerical solution of the Navier-Stokes equations and a single equation turbulence model have achieved some success[1-4] but there are difficulties associated with the specification of a unified length scale over the entire computational domain. Incorporation of higher-order turbulence models and computational resolution of the three-dimensional aspects of the flow field require considerably more time-consuming calculations and have not yet been attempted.

An alternative, component approach,[5-8] proceeds by dividing the flow field into separate interacting regions which are coupled to provide an overall solution. The advantage of this approach is that each region may be represented by models closely related to the physics of the problem and relatively accurate engineering solutions obtained with comparatively simple methods. Within the context of this approach, scaling analyses[8,9] indicate that the details of the impingement region are dominated by a balance of the pressure forces due to flow deflection and the inertial forces of convection.

In this study a variety of incompressible impingement problems are considered under the assumption that the flow within the impingement zone can be treated as an inviscid, rotational flow. Axisymmetric jets impinging normally and two-dimensional jets impinging obliquely form a set of problems that can be formulated in two dimensions with vorticity/radius or vorticity, respectively, conserved along streamlines. Both developing and fully developed jet velocity profiles are considered as entrance conditions to the impingement region and finite difference techniques are used to solve the governing equations. The results are compared with observations in order to determine the range of validity of the inviscid rotational model with respect to the prediction of the ground plane pressure distribution and the structure of the oblique impingement flow field.

Formulation

The normal impingement of axisymmetric jets and the normal/oblique impingement of two-dimensional jets are represented here by the equations governing inviscid rotational flow. The jets are considered to be far from the impingement plane so that influx conditions are not affected by the jet deflection. The formulation is given in terms of dimensionless quantities; velocities are scaled by the maximum jet velocity, distance by the jet half width (i.e., distance measured along the perpendicular from the jet centerline to the point at which the velocity is half the maximum) and pressures by the total pressure at the jet centerline. Ambient and jet static pressure are taken to be zero without loss of generality.

A coordinate system is chosen with z directed perpendicular to the ground plane, positive outward, and x directed along the ground plane such that the origin is at the intersection of the ground plane and the jet centerline (Fig. 1). Eliminating pressure from the x and z momentum equations yields the vorticity equation

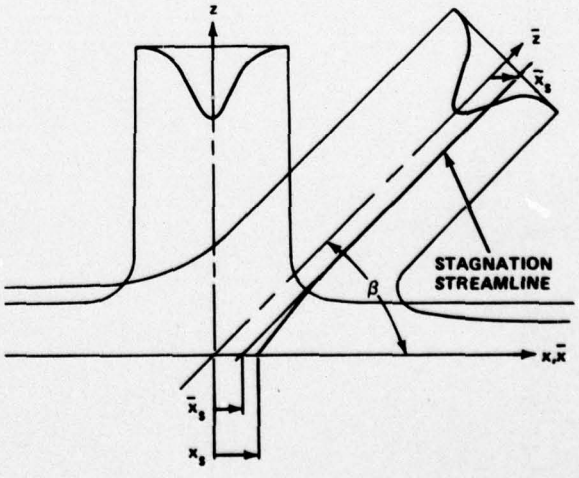

Fig. 1 Schematic of the Jet Impingement Problem

†This investigation was partially supported by the Office of Naval Research under Contract No. N00014-77-C-0524.
*Staff Scientist, Research Department

$$\frac{d(\omega/x^n)}{dt} = u\,\frac{\partial(\omega/x^n)}{\partial x} + w\,\frac{\partial(\omega/x^n)}{\partial z} = 0 \qquad (1)$$

where u and w are the velocities in the x and z directions, respectively, n is an index of the flow character (axisymmetric n = 1, two-dimensional n = 0) and ω is the vorticity defined by

$$\omega = \frac{\partial u}{\partial z} - \frac{\partial w}{\partial x} \ . \qquad (2)$$

A dimensionless stream function

$$\frac{\partial \psi}{\partial x} = - x^n w \ , \quad \frac{\partial \psi}{\partial z} = x^n u \ . \qquad (3)$$

assures satisfaction of mass conservation and when combined with the definition of vorticity produces the Poisson-type equation that provides the basis for the ensuing analysis

$$\frac{\partial^2 \psi}{\partial z^2} + x^n \frac{\partial}{\partial x}\left(\frac{1}{x}\, n\, \frac{\partial \psi}{\partial x}\right) - x^{2n}\left(\frac{\omega}{x^n}\right) = 0 \ . \qquad (4)$$

The unifying feature of the flows considered here is that the vorticity function, ω/x^n, is conserved along stream surfaces and, in the absence of separation bubbles, is fully specified in terms of the incoming jet stream function. The pressure is determined from an auxiliary Bernoulli equation

$$p + u^2 + w^2 = f(\psi) \qquad (5)$$

which follows from the vector momentum equation. This relationship implies that the total pressure is conserved on stream surfaces and completes the formulation of the problem.

Although a unified treatment of the class of flows to be investigated has been presented to this point, it is advantageous to further categorize the flows to more clearly indicate the manner in which boundary conditions are prescribed and special cases are developed. For normal impingement there is flow symmetry about the jet centerline (x = 0) and only the domain $x \geq 0$ need be considered. The boundary conditions are

$\psi(o, z)$	= 0	symmetry	(6a)
$\frac{\partial \psi}{\partial x}(\infty, z)$	= 0	parallel outflow	(6b)
$\psi(x, o)$	= 0	ground plane	(6c)
$\psi(x, \infty)$	= $\psi(x)$	jet inflow	(6d)

The boundary condition at $x \to \infty$ can be replaced by a stream function distribution $\psi(z)$ (e.g., Parameswaren[10]) and it is instructive to demonstrate the relationship between this distribution and condition (6d) as well as the implications of condition (6b).

Consider the points (X, z) for $X \to \infty$ and (x, Z) for $Z \to \infty$ in order to determine a relationship between x and z such that these points lie on the same streamline. The boundary conditions (6b, d) imply that when $X \to \infty$ ($Z \to \infty$) the second (first) term of equation (4) becomes negligible and x and z are related parametrically through $\omega/x^n(\psi)$. For the axisymmetric case, then

$$\left(\frac{1}{X^2}\frac{\partial^2 \psi}{\partial z^2}\right)_X = \left[\frac{1}{x}\frac{\partial}{\partial x}\left(\frac{1}{x}\frac{\partial \psi}{\partial x}\right)\right]_Z \ , \text{ so that}$$

$$\frac{1}{X^2}\left[\frac{\partial^2 \psi}{\partial x^2}\left(\frac{\partial x}{\partial z}\right)^2 + \frac{\partial \psi}{\partial x}\frac{\partial^2 x}{\partial z^2}\right] = \frac{1}{x^2}\frac{\partial^2 \psi}{\partial x^2} - \frac{1}{x^3}\frac{\partial \psi}{\partial x}$$

and, equating coefficients of the stream function derivatives,

$$x\,\frac{\partial^2 x}{\partial z^2} = \frac{\partial}{\partial z}\left(x\,\frac{\partial x}{\partial z}\right) - \left(\frac{\partial x}{\partial z}\right)^2 = -\frac{X^2}{x^2},$$

$$\frac{\partial x}{\partial z} = \frac{X}{x}$$

which has as its solution $x^2 = 2Xz$. Thus, for the axisymmetric case,

$$\psi(X, z) = \psi(\sqrt{2Xz}\,, Z) \qquad (7a)$$

and in a similar fashion it can be shown that for two-dimensional normal impingement

$$\psi(X, z) = \psi(z, Z) \ . \qquad (7b)$$

The boundary condition (6b) can be recovered by noting that

$$\left(\frac{\partial \psi}{\partial x}\right)_X = \left(\frac{\partial \psi}{\partial x}\right)_Z \left(\frac{\partial x}{\partial X}\right)_Z \text{ and, thus,}$$

$$\left(\frac{\partial \psi}{\partial x}\right)_X = 0 \text{ for the two-dimensional case and}$$

$$\left(\frac{\partial \psi}{\partial x}\right)_X = - z\, w(\sqrt{2Xz}\,, Z)$$

for the axisymmetric case. For the velocity profile considered here (Table 1) it can be seen that

$$\left(\frac{\partial \psi}{\partial x}\right)_{X \to \infty} = \frac{z}{(1+2c_2 Xz)^2} \leq \frac{1}{8c_2 X}$$

so that the parallel flow boundary condition is compatible with specification of the far field velocity profile.

Several jet profiles are chosen (Fig. 2) in order to evaluate the effect of fully developed vis a vis developing flow on the ground plane pressure distribution. The functional form of these profiles[11] and the derived stream function distributions and vorticity functions are given in Table 1. The vorticity forcing function is implicitly related to the stream function in the two-dimensional developing jet cases, hence, recasting equation (4) in a new dependent variable $\xi(\psi)$, defined in Table 1, is desirable. For these cases the governing equation becomes

$$\frac{\partial^2 \xi}{\partial x^2} + \frac{\partial^2 \xi}{\partial z^2} + \frac{2}{\sqrt{\pi}}\frac{e^{-\xi^2}}{(1+\mathrm{erf}\,\xi)}\left[\left(\frac{\partial \xi}{\partial x}\right)^2 + \left(\frac{\partial \xi}{\partial z}\right)^2 - \frac{1}{\sigma^2}\right] = 0 \qquad (8)$$

where σ is a spreading parameter for the profiles and the boundary conditions are

$\xi(o, z)$	= $\frac{1}{\sigma}$	(9a)
$\frac{\partial \xi}{\partial x}(\infty, z)$	= 0	(9b)
$\xi(x, o)$	= $\frac{1}{\sigma}$	(9c)
$\xi(x, \infty)$	= $(1-x)/\sigma$	(9d)

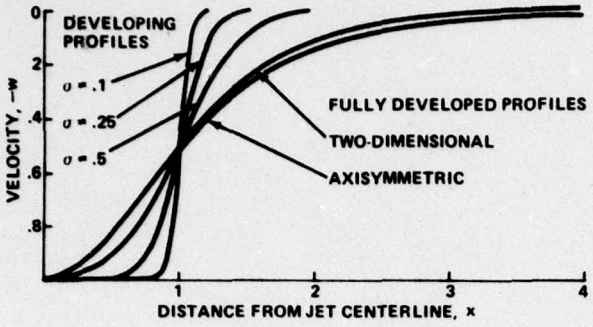

Fig. 2 Jet Velocity Profiles

Equation (4) remains valid for the oblique two-dimensional impingement cases (only fully developed profiles are considered) but the independent variables are transformed so that the new $\bar{z}$ coordinate is aligned with the jet centerline. The new $\bar{x}$ coordinate is measured from the jet centerline in a direction parallel to the ground plane. Therefore,

$$\bar{z} = z/\sin\beta\,,\quad \bar{x} = x - z/\tan\beta \tag{10}$$

and equation (4) becomes

$$\frac{\partial^2\psi}{\partial\bar{x}^2} + \frac{\partial^2\psi}{\partial\bar{z}^2} - 2\cos\beta\,\frac{\partial^2\psi}{\partial\bar{x}\,\partial\bar{z}} + 2c_1^2\sin^2\beta\,\psi(1-c_1^2\psi^2) = 0 \tag{11}$$

where β is the angle between the jet centerline and the ground plane (Fig. 1). The stream function is still related to the velocities u and w by equation (3) and, for $\beta = 90°$, equation (11) reduces to equation (4) with $\bar{x} = x$, $\bar{z} = z$. The boundary conditions for the oblique impingement problem are

$$\frac{\partial\psi}{\partial\bar{x}}(\pm\infty\,,\bar{z}) = 0 \tag{12a,b}$$

$$\psi(\bar{x}\,,\infty) = \frac{1}{c_1}\tanh(c_1\bar{x}\sin\beta) \tag{12c}$$

$$\psi(\bar{x}\,,0) = \psi_s \tag{12d}$$

where ψ_s is the value of the stagnation stream function. It is easily demonstrated that, for the oblique impingement case,

$$\psi(\bar{X}\,,\bar{z}) = \psi(\bar{x}_s + \bar{z}\,,\bar{Z})\ \bar{X}\to\infty,\ \bar{Z}\to\infty \tag{13}$$

where $\bar{x}_s$ is the distance, in the $\bar{x}$ coordinate, from the jet centerline to the stagnation streamline at the jet exit. Using this description of the ground plane flow far from the origin, a balance of momentum in the x direction yields the value for ψ_s. Thus,

$$2\cos\beta\int_0^{\psi_\infty}\bar{w}\,d\psi = \int_{\psi_s}^{\psi_\infty}\bar{u}\,d\psi + \int_{\psi_s}^{\psi_{-\infty}}\bar{u}\,d\psi$$

where $\bar{w}$ and $\bar{u}$ are the velocities in the jet centerline (influx) and ground plane (efflux) directions, respectively. Utilizing the fully developed profile information

$$\text{i.e.,}\ -\bar{w} = \bar{u} = 1 - c_1^2\psi^2\,,\quad \psi_{\pm\infty} = \pm\frac{1}{c_1}$$

produces the desired result

$$\cos\beta = \frac{3}{2}\,c_1\psi_s\,(1-c_1^2\psi_s^2/3) \tag{14}$$

and completes the formulation for the impingement problems considered here.

Method of Solution

Finite difference techniques[10] are used to solve the governing Poisson-type equation for the stream function field. Since the decaying influx and efflux velocity profiles far from the origin are infinite in extent, the calculation of a bounding jet streamline is not of concern. Instead, the extent of the physical domain chosen for the application of the boundary conditions must be large enough that the results in the ground plane are converged (i.e., a larger domain produces no change in results). The normal impingement problem is solved in the rectangular region of height, Z, and width, X (Fig. 3a). Furthermore, to match the stream function at the corner point (X, Z), requires that X = 2Z for the axisymmetric case (Equation 7a) and X = Z for the two-dimensional case (Equation 7b). (Numerical experiments indicate that such a domain produces improved mesh convergence properties.) The oblique impingement problem is solved in the numerically rectangular region of height, $\bar{Z}$, and width, $2\bar{X}$ (Fig. 3b). The displacement of the stagnation streamline, $\bar{x}_s$, is small enough in the problems considered here that at the corner points $(\pm\bar{X},\ \bar{Z})$ the stream function is nearly matched (Equation 13).

Table 1 Rotational Jet Flow Parameters

	Velocity $-w(x)$	Stream Function $\psi(x)$	Vorticity Function $-\omega/x^n(\psi)$
Axisymmetric Fully Developed	$(1 + c_2 x^2)^{-2}$ $c_2 = \sqrt{2} - 1$	$x^2/2(1 + c_2 x^2)$	$4c_2(1 - 2c_2\psi)^3$
Two-Dimensional Fully Developed	$(1 - \tanh^2 c_1 x)$ $c_1 = \tanh^{-1}(1/\sqrt{2})$	$\frac{1}{c_1}\tanh(c_1 x)$	$2c_1^2\psi(1 - c_1^2\psi^2)$
Two-Dimensional Developing	$\frac{1}{2}\{1 + \mathrm{erf}[(1-x)/\sigma]\}$ $\sigma = .1, .25, .5$	$-\frac{\sigma}{2}\int_{1/\sigma}^{(1-x)/\sigma}(1 + \mathrm{erf}\,\xi)\,d\xi$ $\xi = (1 - x)/\sigma$	$\frac{e^{-\xi^2(\psi)}}{\sigma\sqrt{\pi}}$

The numerical representation of equations (4) and (8) makes use of a uniform mesh with spacing defined by

$$\Delta x = \frac{X}{N_X - 1} \quad , \Delta z = \frac{Z}{N_Z - 1}$$

where N_X and N_Z are the number of points in the x and z directions, respectively. Using central differencing for the derivatives of the dependent variable results in the internal point (i, j) finite difference equations for the axisymmetric case (i.e., Equation 4, n = 1),

$$\begin{aligned} &- \psi^*_{i+1,j} + \left[2 + D^2 \left(x_{-j/2} + x_{j/2}\right) \right. \\ &\left. - 8c_2^2 x_{i,j}^2 \left(1 - 2c_2 \psi_{i,j}\right)^2 \right] \psi^*_{i,j} \\ &- \psi^*_{i-1,j} = D^2 \left(x_{j/2} \psi_{i,j+1} + x_{-j/2} \psi_{i,j-1}\right) \\ &+ 4c_2 x_{i,j}^2 \left(1 - 2c_2 \psi_{i,j}^2\right) (\Delta z)^2, \end{aligned} \tag{15}$$

where $D = \Delta z / \Delta x$ and $x_{j/2} = x_{i,j} / (x_{i,j} + \Delta x/2)$, for the two-dimensional fully developed case (i.e., Equation 4, n = 0),

$$\begin{aligned} &- \psi^*_{i+1,j} + \left[2 \left(1 + D^2\right) - 2c_1^2 \left(1 - c_1^2 \psi_{i,j}^2\right) (\Delta z)^2 \right] \psi^*_{i,j} \\ &- \psi^*_{i-1,j} = D^2 \left(\psi_{i,j+1} + \psi_{i,j-1}\right) \end{aligned} \tag{16}$$

and for the two-dimensional developing flow case (i.e., Equation 8),

$$\begin{aligned} &- \left(1 + A_{i,j}\right) \xi^*_{i+1,j} + 2 \left(1 + D^2\right) \xi^*_{i,j} - \left(1 - A_{i,j}\right) \xi^*_{i-1,j} \\ &= D^2 \left(\xi_{i,j+1} + \xi_{i,j-1}\right) + B_{i,j} \left[\frac{D^2}{4} \left(\xi_{i,j+1} - \xi_{i,j-1}\right)^2 \right. \\ &\left. - (\Delta z / \sigma)^2 \right] \end{aligned} \tag{17}$$

where $A_{i,j} = \frac{B_{i,j}}{4} \left(\xi_{i+1,j} - \xi_{i-1,j}\right)$,

$$B_{i,j} = \frac{2}{\sqrt{\pi}} \frac{e^{-\xi_{i,j}^2}}{\left(1 + \operatorname{erf} \xi_{i,j}\right)}.$$

These equations are modified slightly at x = X by the use of additional fictitious points to satisfy the gradient boundary condition by reflection. The equations (15-17) are arranged for line relaxation by tridiagonal solution techniques. The asterisk superscript refers to an intermediate value of the dependent variable; coefficients of these variables and the right sides of the equations refer to previous values of these quantities (i.e., ν^{th} iterative values). The $(\nu+1)$ values are obtained by the relaxation formula (18)

$$\psi^{\nu+1}_{i,j} = (1 - r) \psi^{\nu}_{i,j} + r \, \psi^*_{i,j} \tag{18}$$

where $0 < r < 1$ indicates under-relaxation and $1 < r < 2$ indicates over-relaxation. The nonlinear vorticity forcing functions have been arranged in equations (15-17) so that they are partially included in the implicit line relaxation calculation.

A similar representation of equation (11), for oblique impingement, makes use of a uniform mesh with spacings

$$\Delta \bar{x} = \frac{2\bar{X}}{N_{2\bar{X}} - 1} \, , \Delta \bar{z} = \frac{\bar{Z}}{N_{\bar{Z}} - 1}$$

where $N_{2\bar{X}}$ and $N_{\bar{Z}}$ are the number of points in the $\bar{X}$ and $\bar{Z}$ directions, respectively and yields the internal point finite difference equation

$$\begin{aligned} &- \psi^*_{i+1,j} + 2 \left[1 + \bar{D}^2 - c_1^2 \left(1 - c_1^2 \psi_{i,j}^2\right) \right. \\ &\left. \sin^2 \beta (\Delta z)^2 \right] \psi^*_{i,j} - \psi^*_{i-1,j} \\ &= \bar{D}^2 \left(\psi_{i,j+1} + \psi_{i,j-1}\right) - \frac{\bar{D}}{2} \cos \beta \left(\psi_{i+1,j+1} + \psi_{i-1,j-1} \right. \\ &\left. - \psi_{i+1,j-1} - \psi_{i-1,j+1}\right) \end{aligned} \tag{18}$$

where $\bar{D} = \Delta \bar{z} / \Delta \bar{x}$.

The ground plane velocity is a derived quantity of considerable importance since it determines the ground plane pressure by Bernoulli's equation. From equation (3), and the appropriate transformations, this velocity is given, to second order in mesh height, by

$$u(o, x) = \left[\psi(x, \Delta z) - \frac{1}{2} \frac{\partial^2 \psi}{\partial z^2} (x, o) (\Delta z)^2\right] / x^n \Delta z \tag{19a}$$

for fully developed normal impingement, by

$$u(o, x) = \frac{1}{2} \left(1 + \operatorname{erf} \frac{1}{\sigma}\right) \left[1 - \sigma \xi (x, \Delta z)\right] / \Delta z \tag{19b}$$

for the normal impingement developing flow and by

$$\begin{aligned} u(o, \bar{x}) = &- \left[\psi(\bar{x}, \Delta \bar{z}) - \psi_s \right. \\ &\left. - \frac{1}{2} \frac{\partial^2 \psi}{\partial \bar{z}^2} (\bar{x}, o) (\Delta \bar{z})^2\right] / \Delta \bar{z} \sin \beta \end{aligned} \tag{19c}$$

for two-dimensional oblique impingement. The value of the second derivative of the stream function can be found from the governing differential equations evaluated at the ground plane. For the fully developed normal impingement cases this is easily done $\left(\frac{\partial^2 \psi}{\partial z^2} = 0 \text{ in 2D flow}, \quad \frac{\partial^2 \psi}{\partial z^2} = x\omega \text{ in axisymmetric flow}\right)$. The oblique impingement case, however, requires calculation of a row of coupled fictitious points located at $\bar{z} = -\Delta \bar{z}$ (via Equation 18) in order to represent the stream function second derivative,

$$\begin{aligned} \text{i.e.,} \frac{\partial^2 \psi}{\partial \bar{z}^2} (\bar{x}, o) = &\left[\psi(\bar{x}, \Delta \bar{z}) - 2\psi_s \right. \\ &\left. + \psi(x, -\Delta \bar{z})\right] / (\Delta \bar{z})^2. \end{aligned}$$

The ground plane pressure is evaluated from

$$p(\bar{x}, o) = u^2 (\bar{x}_s, \bar{Z}) - u^2(\bar{x}, o). \tag{20}$$

A considerable number of calculations are necessary (e.g., Table 2) in order to determine the character of the numerical solution. Initial estimates for all

Table 2 Numerical parameters for selected impingement computations.

	Axisymmetric	Two-Dimensional									
	Normal	Normal				Oblique (Fully Developed)					
			σ			β (deg)					
	Fully Developed	Fully Developed	.5	.25	.1	80	70	60	50	40	30
$X(2\bar{X})$*	8	5	5	5	5	10	10	12	12	16	20
$Z(\bar{Z})$	4	5	5	5	5	5	5	6	6	8	10
$N_X(N_{2\bar{X}})$	81	41	41	41	41	41	41	81	41	41	41
$N_Z(N_{\bar{Z}})$	161	41	41	41	41	21	21	41	21	21	21
ϵ	10^{-6}	10^{-6}	10^{-5}	10^{-5}	10^{-5}	10^{-6}	10^{-6}	10^{-6}	10^{-6}	10^{-6}	10^{-6}
ν	438	370	338	428	1938	741	816	3401	1063	1435	1799

*Quantities in parentheses refer to the oblique impingement caes
X = width, Z = height, N = number of points, ϵ = tolerance, ν = number of iterations

computations reported here are obtained by linear interpolation between the ground and jet exit stream function conditions. The successive relaxation procedure (Equation 18) is applied until a convergence given by

$$\psi_{i,j}^{\nu+1} - \psi_{i,j}^{\nu} \leq \epsilon |\psi_{i,j}^{\nu}|_{\max} \tag{21}$$

is obtained. It is found that the convergence parameter $\epsilon = 10^{-5}$ is sufficient so that when ϵ is reduced by an order of magnitude the maximum velocity variation at a ground plane point is less than 10^{-3}.

The domains of integration and mesh widths indicated in Table 2 for fully developed normal impingement reproduce the parallel flow conditions at x = X (i.e., Equations (7a,b) are satisfied). It can be shown that the criterion $(X\Delta z)^2 << 1$ must be satisfied in addition to condition (7a) in order for the axisymmetric ground plane velocity to achieve its asymptotic value, $u(X,0) \to 1$. The case tabulated, for example, has a slight overshoot in velocity beginning at x = 3.7 and reaching a maximum of 1.6% at x = X = 8.

As might be expected from a glance at Fig. 2, the developing flow cases are the most difficult to compute. The resolution of the jet velocity profiles with a uniform mesh becomes impractical for spreading parameters, $\sigma \leq 0.1$. Furthermore, the nature of the variable, ξ, is such that it grows negatively without bound as the width of the numerical domain is increased. A cut-off, such that $\xi \geq -3.49$, is used to restrict this growth and only points satisfying this criterion are considered within the domain governed by equation (17). This procedure, along with appreciable under-relaxation (e.g., r = 0.3 for $\sigma = 0.1$), provides converged solutions which recover the asymptotic ground plane velocity even for the smallest spreading parameter (i.e., u(0,X) = 0.98 at $\sigma = 0.1$).

Convergence in the oblique impingement case requires a domain that increases as the inclination angle, β, departs from 90°. Numerical experiments indicate that $\bar{Z} = 5/\sin\beta$ and $X = \bar{Z}$ (from Equation 13) provides an adequate domain for these computations. The mesh width convergence at $\beta = 60°$ is such that a 41 x 21 grid produces ground plane velocities within 1% of those predicted by an 81 x 41 grid. A similar result is found for the normal impingement case. In order to further estimate the convergence properties of the oblique impingement cases of Table 2, the resultant force on the ground plane and the moment about the origin are computed from the numerical distribution of the ground plane pressure and compared with their exact values assuming recovery of the initial profiles at large $\bar{X}$ (i.e., Equation 13 is satisfied). Thus,

$$F(\text{calc}) = \frac{1}{2}\int_{-\bar{X}}^{\bar{X}} p\, d\bar{x},$$

$$F(\text{exact}) = -2\sin\beta \int_0^{\psi_\infty} \bar{w}\, d\psi \tag{22}$$

$$M_o(\text{calc}) = \frac{1}{2}\int_{-\bar{X}}^{\bar{X}} p\bar{x}\, d\bar{x}, \tag{23}$$

$$M_o(\text{exact}) = \bar{x}_s\, F(\text{exact}).$$

From a moment balance about $\bar{x}_s$, the location of the resultant force, it can be seen by inspection that $\bar{x}_s$ is also the distance from the jet centerline to the stagnation streamline measured at the jet exit and along the direction parallel to the ground plane (Fig. 1).

It is demonstrated (Table 3) that the computed force and moment are in error by at most 3% and 2%, respectively, indicating that the oblique impingement cases are sufficiently converged.

The computations require about 10^{-3} seconds/iteration/(number of points) and have been performed using an HP 3000 Series II computing system (a factor of about 20 relates this time to IBM 370-168 time). Few experiments have been done to optimize the relaxation parameter; the cases of Table 2, except for the developing profiles, used r = 1. The cases listed in Table 2 are those used to demonstrate convergence properties and quite satisfactory solutions can be obtained for many of the cases with considerably less stringent conditions. Finally, although the cases presented here include impingement angles down to 30°, the limitation is on physical rather than numerical grounds; converged computations have been established for β as low as 10°.

Table 3 Comparison of computed and exact ground plane force and moment as a function of impingement angle.

β	F (calc)	F (exact)	M_O (calc)	M_O (exact)
80°	1.535	1.490	-.1972	-.2005
70°	1.456	1.422	-.3958	-.4059
60°	1.321	1.310	-.6120	-.6219
50°	1.170	1.159	-.8360	-.8563
40°	0.977	0.972	-1.140	-1.121
30	0.750	0.756	-1.462	-1.436

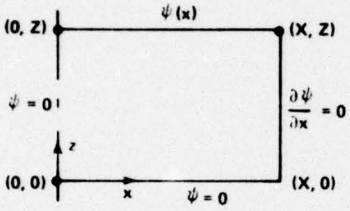

a) Normal Impingement

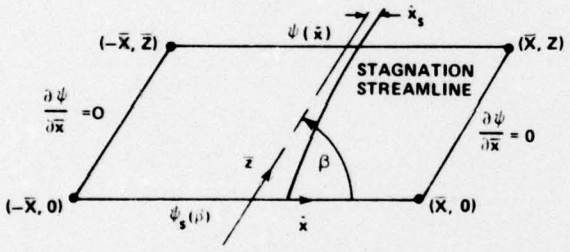

b) Oblique Impingement

Fig. 3 Physical Domain and Boundary Conditions for Finite Difference Analysis

Results and Discussion

The computations described here are for idealized inviscid rotational jets located far from the impingement plane with lengths scaled by the jet half width and pressures by the maximum jet total pressure. Real jets, however, encounter a free mixing zone prior to entry into the impingement region and data are usually presented with length scales given by either the jet height above ground or the half width of the undisturbed jet at the ground plane. If a matching point between the computed solution and point of free jet entry to the impingement zone is established then the free jet length scales can be related to the computational length scale by well known free jet spreading rate parameters[9,12,13]. In presenting the computation/data comparisons it is convenient to use the rotational jet length scale so that dimensionless jet heights, h, are always referred to this quantity. The ground pressure data are normalized by the peak ground plane pressure, p_m, to eliminate total pressure loss considerations.

For normal axisymmetric impingement, Giralt et al. use the criterion that the impingement region commences when the centerline velocity is 98% of that in the undisturbed free jet at the identical distance from the nozzle exit. According to the present computations the location of this point is at $z \simeq 2.1$ which is in close agreement with the value, $z \simeq 2.2$ observed by Giralt et al. Comparison of the calculated ground plane pressure distribution with data[9,12] (Fig. 4) shows excellent agreement over the entire range of the distribution. This is a considerable improvement upon the inviscid solution of Scholtz and Trass[13] which breaks down at large distances from the centerline. The agreement between the current computations and those of Scholtz and Trass for velocity decay along the centerline is demonstrated in Fig. 5: the discrepancy with respect to the data[13,14] is attributed to mixing phenomena within the impingement zone[12].

Comparison of the results for the normal impingement of fully developed two-dimensional jets proceeds in a similar manner. Numerical computations yield the 98% criterion at $z \simeq 3.46$ which, in conjunction with accepted spreading rates[11], provides the relationship $h \simeq 12.2$, where, again, h is the dimensionless distance from the jet exit to the ground plane. The calculations, (Fig. 6), indicate that for this case, too, there is excellent agreement with observations.

If the jet exit plane is in proximity to the ground plane (but outside the impingement zone), then a core region is present and a developing velocity profile

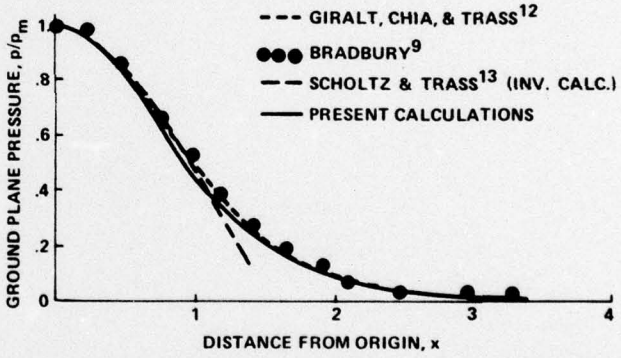

Fig. 4 Ground Plane Pressure Distribution, Axisymmetric Normal Impingement

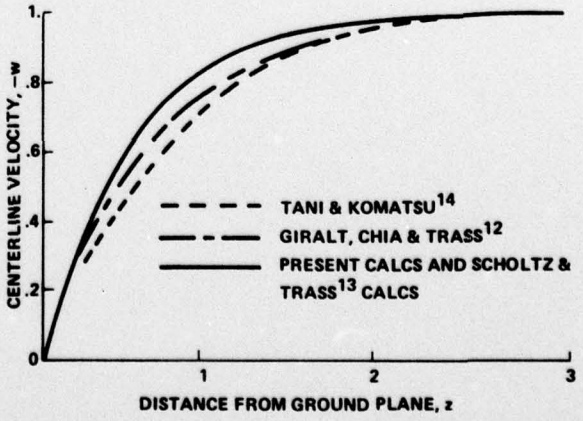

Fig. 5 Centerline Velocity Decay, Axisymmetric Normal Impingement

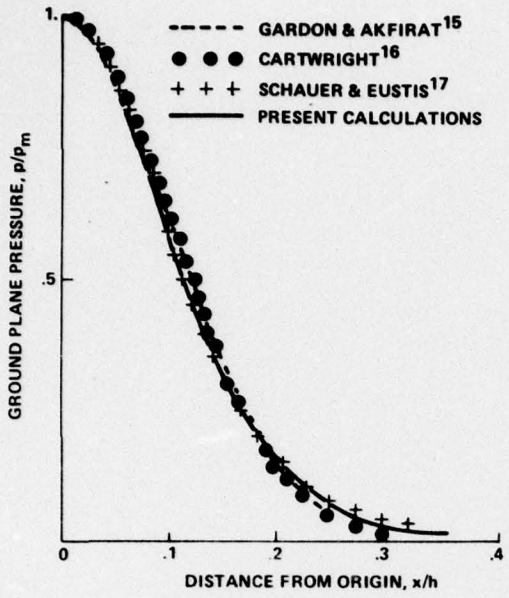

Fig. 6 Ground Plane Pressure Distributions Two-Dimensional Normal Impingement, Fully Developed Jet Profile

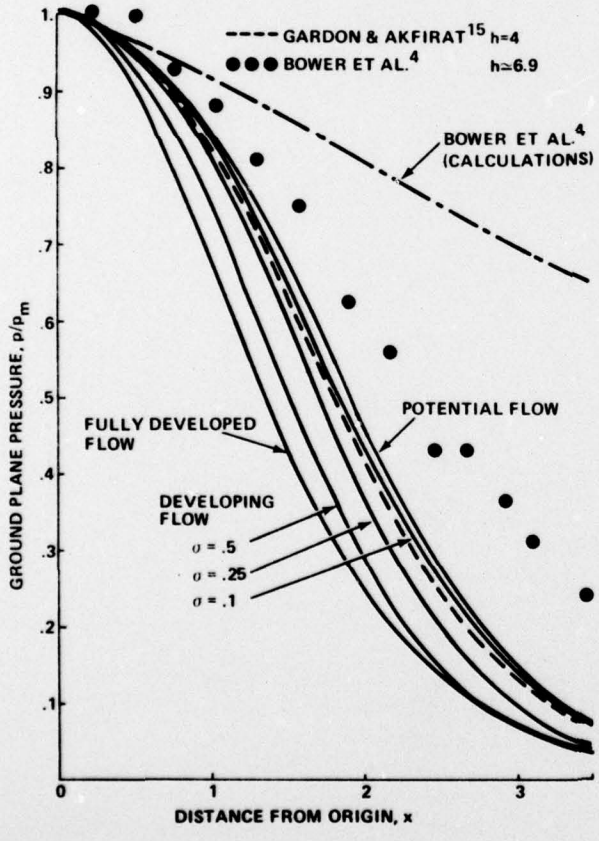

Fig. 7 Ground Plane Pressure Distribution, Two-Dimensional Normal Impingement, Fully Developed and Developing Jet Profiles

exists at the beginning of the impingement zone. The computations of ground plane pressures under such conditions are shown in Fig. 7 and are seen to fall between the potential flow solution[18] and the fully developed rotational flow solution. A comparison with the data of Gardon and Akfirat,[16] assuming that the half width is half the jet width (i.e., core flow is present), shows that the measured ground plane pressures are between the computed developing flow cases $\sigma = .1$ and $\sigma = .25$. Qualitatively similar results are found in the axisymmetric case when data[12,19] are compared with the potential flow solution of Strand.[20] From Bower et al.'s[4] data, obtained with a curved confining plate around the two-dimensional jet exit, the half width at the impingement zone is estimated to be 1.16 jet widths, in reasonable agreement with the assumption of a developing flow. Although the ground plane pressure data differ from the present calculations, a solution to the full Navier-Stokes equations by Bower et al.[4] shows no improvement (Fig. 7). The confining plate, which can be the source of the discrepancy vis a vis the inviscid calculations, is not expected to influence the results near the centerline.[21] Fig. 8 demonstrates that the centerline velocity decay is closely represented by the developing flow case, $\sigma \simeq 0.5$, while the Navier-Stokes representation[4] still produces poor results.

Computation of two-dimensional, oblique impingement produces the flow configurations depicted in Fig. 9. As the jet inclination angle, β, decreases from 90° the stagnation streamline shifts, according to Equation (14) in order to maintain the momentum balance. This shift reduces the total pressure of the stagnation streamline (Fig. 10), although the pressure distributions still appear to be symmetric about the peaks. The calculations show (Fig. 9) that for fully developed jets, the stagnation streamlines approach the ground plane with virtually no deflection. A Taylor series expansion of the stream function about the stagnation point shows that the stagnation line incidence angle, β_s, is related to the velocity gradient at the stagnation point, $(\partial u/\partial x)_s$, and the jet vorticity distribution by

$$\tan \beta_s = -\frac{2(\partial u/\partial x)_s}{\omega(x_s)}, \qquad (24)$$

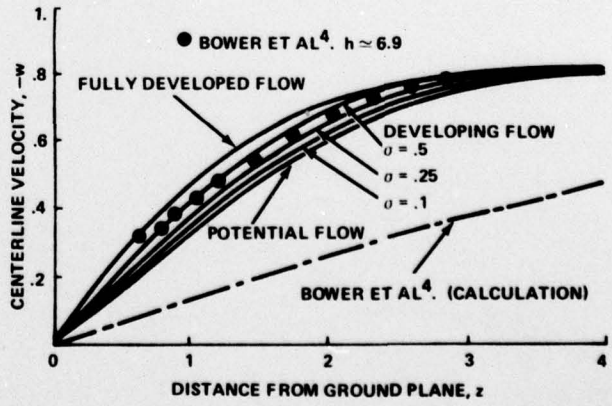

Fig. 8 Centerline Velocity Decay, Two Dimensional Normal Impingement, Fully Developed, Developing Jet Profiles

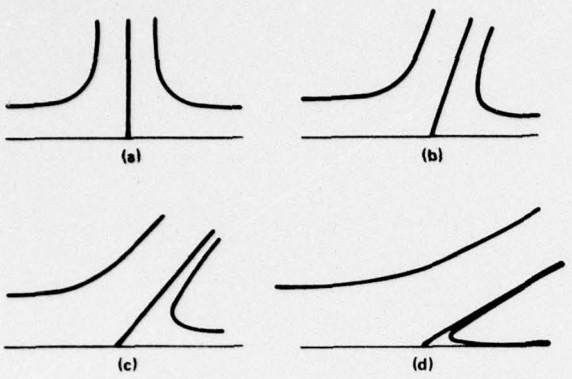

Fig. 9 Computations of Jet Half width and Stagnation Streamlines (a) $\beta = 90°$, (b) $\beta = 70°$, (c) $\beta = 50°$, (d) $\beta = 30°$

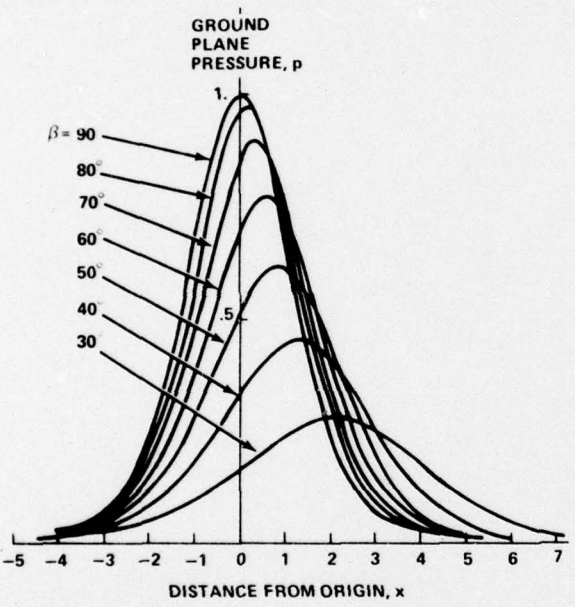

Fig. 10 Fully Developed Flow Ground Plane Pressure Distribution Computations for 2-D Oblique Jet Impingement

where $\omega(x_s)$ is the vorticity on the stagnation streamline. This relationship which is well satisfied in the numerical calculations serves to verify the computational results and indicates that for a uniform (potential) jet the stagnation streamline is perpendicular to the ground plane. It is instructive to compare further the rotational and potential jet cases. The location, $\bar{x}_s$, of the resultant force is almost identical for the two cases over the range $30° \lesssim \beta \leq 90°$ but the deflection of the uniform jet stagnation streamline causes a significant displacement of the maximum pressure point[22], x_s, whereas $\bar{x}_s$ and x_s are virtually coincident for the fully developed jet (Fig. 11). The separation, $x_s - \bar{x}_s$, implies a ground plane pressure distribution[18] that is asymmetric about the stagnation point (Fig. 12) in contrast to the result for the fully developed jet.

The data of Schauer and Eustis[17] is compared with the present computations for the fully developed jet by again relating jet heights and half widths (Table 4). The observed stagnation point location (Fig. 11) is in agreement with the computations at $\beta = 70°$ but deviates with reduced impingement angles. Included in the calculated results is a case with $\beta = 20°$ in order to illustrate that the magnitude of the observed trends are recovered by the computations.

Table 4 Dimensionless jet impingement zone height, $\bar{z}$, and free jet exit plane height, $\bar{h}$, measured from the ground plane along the jet centerline as a function of impingement angle.

β(deg)	$\bar{z}$	$\bar{h}$	$\bar{z}/\bar{h}$
90	3.46	12.2	.28
80	3.51	12.2	.28
70	3.57	12.3	.29
60	3.83	12.5	.31
50	4.13	12.8	.32
40	4.84	13.5	.36
30	5.78	14.5	.40

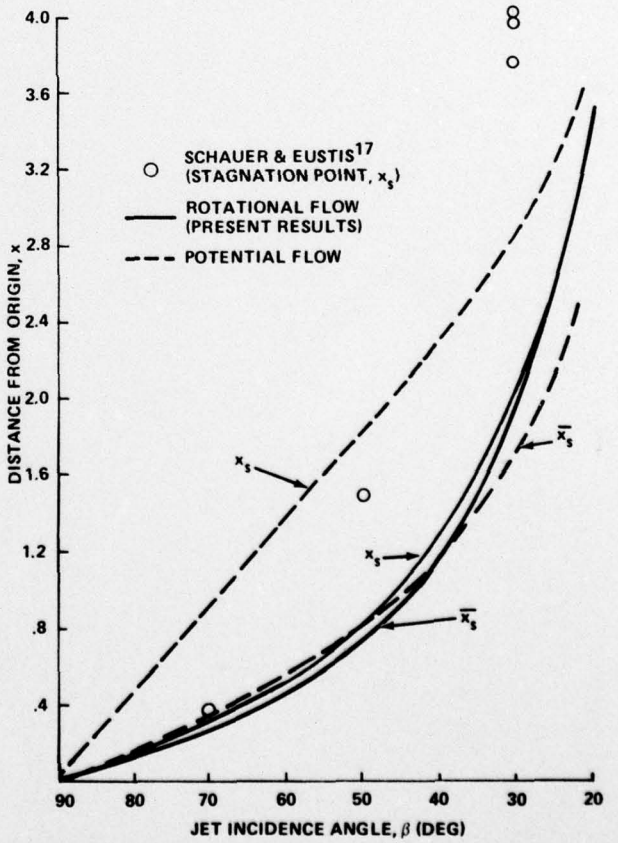

Fig. 11 Ground Plane Location of Resultant Force and Stagnation Point for Rotational, Irrotational Jets ($\bar{x}_s$, Resultant Force; x_s, Stagnation Point)

The ground plane pressure distribution data exhibit symmetry about the stagnation point as suggested earlier and are well represented by the calculations for $60° \lesssim \beta \leq 90°$ (Fig. 13). This is consistent with the range over which agreement is obtained for the location of the stagnation point. Quantitative disagreement between the computations and data at more shallow incidence angles is not unexpected. The calculated height of the impingement zone is 40% of the jet height at $\beta = 30°$ (Table 4) which, along with order of magnitude arguments that can be invoked,[9,23] illustrates the increasing influence of the turbulent stress gradient terms and consequent breakdown of the inviscid rotational flow model at shallow impingement angles.

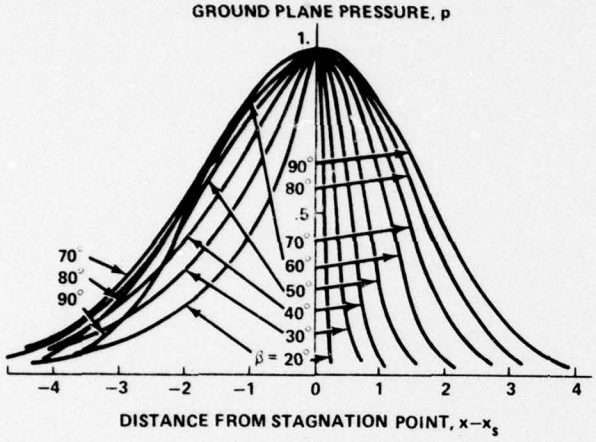

Fig. 12 Potential Flow Ground Plane Pressure Distribution for 2-D Oblique Jet Impingement

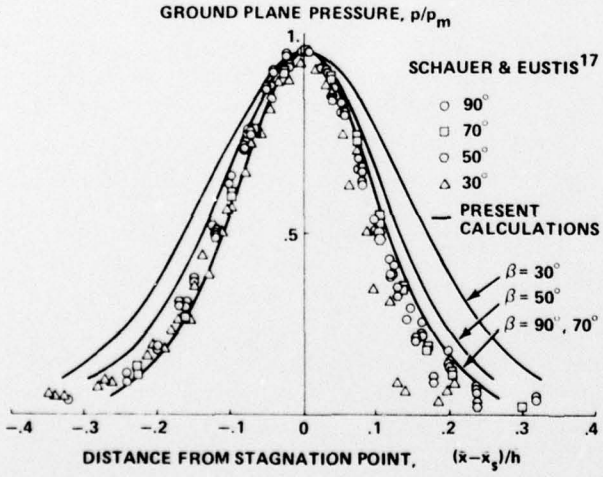

Fig. 13 Comparison of Computed and Observed Ground Plane Pressure Distributions for 2-D Oblique Impingement

Conclusions

Numerical computations for a variety of rotational jet impingement problems are given here. From the results and discussion it may be concluded that:

(1) the inviscid rotational flow formulation provides an excellent description of the ground plane pressure distribution for normally impinging fully developed axisymmetric and two-dimensional jets,

(2) ground plane pressure distributions and centerline velocity decays for normally impinging developing two-dimensional jets may also be represented by this technique and show improvement with respect to existing Navier-Stokes type computations,

(3) the structure of obliquely impinging fully developed two-dimensional jets is such that the stagnation streamline exhibits little deflection and the ground plane pressure distributions are symmetric about the stagnation point,

(4) quantitative agreement with observations is obtained for stagnation point location and ground plane pressure distribution for oblique jet impingement angles $\beta \gtrsim 60°$, and

(5) the extent of the impingement zone increases as the jet inclination angle drops (e.g., at $\beta = 30°$ it is 40% of the jet height) providing one indication that turbulent stress gradient terms become increasingly relevant in the impingement zone for $\beta \lesssim 60°$.

Acknowledgement

The author is indebted to Drs. R. Melnik and S. Rudman for suggesting this problem.

References

1. Wolfshtein, M., "Some Solutions of the Plane Turbulent Impinging Jet," J. Basic Eng., Trans. ASME, 92D, 915, 1970.

2. Bower, W. W. and Kotansky, D. R., "A Navier-Stokes Analysis of the Two-Dimensional Ground Effects Problem," AIAA Paper No. 76-621, AIAA/SAE 12th Propulsion Conference, Palo Alto, Cal., July 26-29, 1976.

3. Kotansky, D. R. and Bower, W. W., "A Basic Study of the VTOL Ground Effect Problem for Planar Flow," AIAA Paper No. 77-614, AIAA/NASA Ames V/STOL Conference, Palo Alto, Cal., June 6-8, 1977.

4. Bower, W. W., Kotansky, D. R. and Hoffman, G. H., "Computations and Measurements of Two-Dimensional Turbulent Jet Impingement Flowfields, "Symposium on Turbulent Shear Flows, Vol. 1, University Park, PA., April 18-20, 1977.

5. Siclari, M. J., Migdal, D. and Palcza, J. L., "The Development of Theoretical Models for Jet-Induced Effects on V/STOL Aircraft, "J. Aircraft, 13, 938, 1976.

6. Siclari, M. J., Hill, W. G., Jr. and Jenkins, R. C., "Investigation of Stagnation Line and Upwash Formation," AIAA Paper No. 77-615, AIAA/NASA Ames V/STOL Conference, Palo Alto, Cal., June 6-8, 1977.

7. Siclari, M. J., Aidala, P., Wohllebe, F. and Palcza, J. L., "Development of Prediction Techniques for Multi-Jet Thermal Ground Flow Field and Fountain Formation," AIAA Paper No. 77-616, AIAA/NASA Ames V/STOL Conference, Palo Alto, Cal., June 6-8, 1977.

8. Sparrow, E. M. and Lee, L., "Analysis of Flow Field and Impingement Heat/Mass Transfer Due to a Nonuniform Slot Jet," J. Heat Trans, Trans. ASME, 97C, 191, 1975.

9. Bradbury, L. J. S., "The Impact of an Axisymmetric Jet onto a Normal Ground," Aeronautical Quart., 23, 141, 1972.

10. Parameswaren, V. and Alpay, S. A., "Normal Impingement of Jets," J. Aircraft, 13, 189, 1974.

11. Schlichting, H., Boundary Layer Theory, 4th ed., Chapter XXIII, McGraw-Hill Book Company, Inc, New York, 1960.

12. Giralt, F., Chia, C. J. and Trass, O., "Characterization of the Impingement Region in an Axisymmetric Turbulent Jet," Ind. Eng. Chem., Fundam., 16, 21, 1977.

13. Scholtz, M. T. and Trass, O., "Mass Transfer in a Nonuniform Impinging Jet Part 1. Stagnation Flow-Velocity and Pressure Distribution," AIChE J., 16, 82, 1970.

14. Tani, I. and Komatsu, Y., " Impingement of a Round Jet on a Flat Plate," Eleventh Int'l Conf. of Appl. Mech., Munich, 1964. Springer-Verlag, Berlin, 1966.

15. Gardon, R. and Akfirat, J. C., " The Role of Turbulence in Determining the Heat-Transfer Characteristics of Impinging Jets," Int. J. Heat and Mass Trans., 8, 1261, 1965.

16. Cartwright, W. G. and Russell, P. J., " Characteristics of a Turbulent Slot Jet Impinging on a Plane Surface," Paper No. 32, Thermodynamics and Fluid Mechanics Convention, Inst. of Mech. Engineers, Bristol, England, Mar. 27-29, 1968.

17. Schauer, J. J. and Eustis, R. H., "The Flow Development and Heat Transfer Characteristics of Plane Turbulent Impinging Jets," TR 3, Department of Mechanical Engineering, Standard University, Sept., 1963

18. Milne-Thomson, L. M., Theoretical Hydrodynamics, 4th ed., Chapter XI, The Macmillan Company, New York, 1960.

19. Hill, W. G., Jr. and Jenkins, R. C., "Experimental Investigation of Mulitple Jet Impingement Flows Applicable to VTOL Aircraft in Ground Effect," Grumman Research Dept, RM-605, 1975.

20. Strand, T., "On the Theory of Normal Ground Impingement of Axi-Symmetric Jets in Inviscid Incompressible Flow," AIAA Paper No. 64-424, 1964.

21. Saad, N. R., Douglas, W. J. M. and Mujumdar, A. S., "Prediction of Heat-Transfer under an Axisymmetric Laminar Impinging Jet," Ind. Eng. Chem., Fundam, 16, 148, 1977.

22. Slezkin, N. A., "On Impact of a Plane Gas Stream Upon an Infinite Wall," Prikladnaia Matematika I Mekhanika, 16, 227, 1952.

23. Foss, J. F. and Kleiss, S. J., "The Oblique Impingement of an Axisymmetric Jet," Proc. Fourth Canadian Congr. of Applied Mech., Montreal, May 28 - June 1, 1973.

DISTRIBUTION LIST FOR UNCLASSIFIED
TECHNICAL REPORTS AND REPRINTS ISSUED UNDER
CONTRACT N00014-77-C-0524 TASK NR061-251

All addresses receive one copy unless otherwise specified

Technical Library
Building 313
Ballistic Research Laboratories
Aberdeen Proving Ground, MD 21005

Dr. F. D. Bennett
External Ballistic Laboratory
Ballistic Research Laboratories
Aberdeen Proving Ground, MD 21005

Mr. C. C. Hudson
Sandia Corporation
Sandia Base
Albuquerque, NM 81115

Professor P. J. Roache
Ecodynamics Research
Associates, Inc.
P. O. Box 8172
Albuquerque, NM 87108

Dr. J. D. Shreve, Jr.
Sandia Corporation
Sandia Base
Albuquerque, NM 81115

Defense Documentation Center
Cameron Station, Building 5
Alexandria, VA 22314 12 copies

Library
Naval Academy
Annapolis, MD 21402

Director, Tactical Technology Office
Defense Advanced Research Projects
Agency
1400 Wilson Boulevard
Arlington, VA 22209

Office of Naval Research
Attn: Code 211
800 N. Quincy Street
Arlington, VA 22217

Office of Naval Research
Attn: Code 438
800 N. Quincy Street
Arlington, VA 22217

Office of Naval Research
Attn: Code 1021P (ONRL)
800 N. Quincy Street
Arlington, VA 22217 6 copies

Dr. J. L. Potter
Deputy Director, Technology
von Karman Gas Dynamics Facility
Arnold Air Force Station, TN 37389

Professor J. C. Wu
Georgia Institute of Technology
School of Aerospace Engineering
Atlanta, GA 30332

Library
Aerojet-General Corporation
6352 North Irwindale Avenue
Azusa, CA 91702

NASA Scientific and Technical
Information Facility
P. O. Box 8757
Baltimore/Washington International
Airport, MD 21240

Dr. K. C. Wang
Martin Marietta Corporation
Martin Marietta Laboratories
1450 South Rolling Road
Baltimore, MD 21227

Dr. S. A. Berger
University of California
Department of Mechanical Engineering
Berkeley, CA 94720

Professor A. J. Chorin
University of California
Department of Mathematics
Berkeley, CA 94720

Professor M. Holt
University of California
Department of Mechanical Engineering
Berkeley, CA 94720

Dr. H. R. Chaplin
Code 1600
David W. Taylor Naval Ship Research
and Development Center
Bethesda, MD 20084

Dr. Hans Lugt
Code 184
David W. Taylor Naval Ship Research
and Development Center
Bethesda, MD 20084

Dr. Francois Frenkiel
Code 1802.2
David W. Taylor Naval Ship Research
and Development Center
Bethesda, MD 20084

Dr. G. R. Inger
Department of Aerospace Engineering
Virginia Polytechnic Institute and
State University
Blacksburg, VA 24061

Professor A. H. Nayfeh
Department of Engineering Science
Virginia Polytechnic Institute and
State University
Blacksburg, VA 24061

Mr. A. Rubel
Research Department
Grumman Aerospace Corporation
Bethpage, NY 11714

Commanding Officer
Office of Naval Research Branch Office
666 Summer Street, Bldg. 114, Section D
Boston, MA 02210

Dr. G. Hall
State University of New York at Buffalo
Faculty of Engineering and Applied
Sciences
Fluid and Thermal Sciences Laboratory
Buffalo, NY 14214

Dr. R. J. Vidal
CALSPAN Corporation
Aerodynamics Research Department
P. O. Box 235
Buffalo, NY 14221

Professor R. F. Probstein
Department of Mechanical Engineering
Massachusetts Institute of Technology
Cambridge, MA 02139

Commanding Officer
Office of Naval Research Branch Office
536 South Clark Street
Chicago, IL 60605

Code 753
Naval Weapons Center
China Lake, CA 93555

Mr. J. Marshall
Code 4063
Naval Weapons Center
China Lake, CA 93555

Professor R. T. Davis
Department of Aerospace Engineering
University of Cincinnati
Cincinnati, OH 45221

Library MS 60-3
NASA Lewis Research Center
21000 Brookpark Road
Cleveland, OH 44135

Dr. J. D. Anderson, Jr.
Chairman, Department of Aerospace
Engineering
College of Engineering
University of Maryland
College Park, MD 20742

Professor W. L. Melnik
Department of Aerospace Engineering
University of Maryland
College Park, MD 20742

Professor O. Burggraf
Department of Aeronautical and
Astronautical Engineering
Ohio State University
1314 Kinnear Road
Columbus, OH 43212

Technical Library
Naval Surface Weapons Center
Dahlgren Laboratory
Dahlgren, VA 22448

Dr. F. Moore
Naval Surface Weapons Center
Dahlgren Laboratory
Dahlgren, VA 22448

Technical Library 2-51131
LTV Aerospace Corporation
P. O. Box 5907
Dallas, TX 75222

Library, United Aircraft Corporation
Research Laboratories
Silver Lane
East Hartford, CT 06108

Technical Library
AVCO-Everett Research Laboratory
2385 Revere Beach Parkway
Everett, MA 02149

Professor G. Moretti
Polytechnic Institute of New York
Long Island Center
Department of Aerospace Engineering
and Applied Mechanics
Route 110
Farmingdale, NY 11735

Professor S. G. Rubin
Polytechnic Institute of New York
Long Island Center
Department of Aerospace Engineering
and Applied Mechanics
Route 110
Farmingdale, NY 11735

Dr. W. R. Briley
Scientific Research Associates, Inc.
P. O. Box 498
Glastonbury, CT 06033

Professor P. Gordon
Calumet Campus
Department of Mathematics
Purdue University
Hammond, IN 46323

Library (MS 185)
NASA Langley Research Center
Langley Station
Hampton, VA 23665

Professor A. Chapmann
Chairman, Mechanical Engineering
Department
William M. Rice Institute
Box 1892
Houston, TX 77001

Technical Library
Naval Ordnance Station
Indian Head, MD 20640

Professor D. A. Caughey
Sibley School of Mechanical and
Aerospace Engineering
Cornell University
Ithaca, NY 14850

Professor E. L. Resler
Sibley School of Mechanical and
Aerospace Engineering
Cornell University
Ithaca, NY 14850

Professor S. F. Shen
Sibley School of Mechanical and
Aerospace Engineering
Ithaca, NY 14850

Library
Midwest Research Institute
425 Volker Boulevard
Kansas City, MO 64110

Dr. M. M. Hafez
Flow Research, Inc.
P. O. Box 5040
Kent, WA 98031

Dr. E. M. Murman
Flow Research, Inc.
P. O. Box 5040
Kent, WA 98031

Dr. S. A. Orszag
Cambridge Hydrodynamics, Inc.
54 Baskin Road
Lexington, MA 02173

Dr. P. Bradshaw
Imperial College of Science and
Technology
Department of Aeronautics
Prince Consort Road
London SW7 2BY, England

Professor T. Cebeci
California State University,
LongBeach
Mechanical Engineering Department
Long Beach, CA 90840

Mr. J. L. Hess
Douglas Aircraft Company
3855 Lakewood Boulevard
Long Beach, CA 90808

Dr. H. K. Cheng
University of Southern California,
University Park
Department of Aerospace Engineering
Los Angeles, CA 90007

Professor J. D. Cole
Mechanics and Structures Department
School of Engineering and Applied
Science
University of California
Los Angeles, CA 90024

Engineering Library
University of Southern California
Box 77929
Los Angeles, CA 90007

Dr. C. -M. Ho
Department of Aerospace Engineering
University of Southern California,
University Park
Los Angeles, CA 90007

Dr. T. D. Taylor
The Aerospace Corporation
P. O. Box 92957
Los Angeles, CA 90009

Commanding Officer
Naval Ordnance Station
Louisville, KY 40214

Mr. B. H. Little, Jr.
Lockheed-Georgia Company
Department 72-74, Zone 369
Marietta, GA 30061

Professor E. R. G. Eckert
University of Minnesota
241 Mechanical Engineering Building
Minneapolis, MN 55455

Library
Naval Postgraduate School
Monterey, CA 93940

Supersonic-Gas Dynamics Research
Laboratory
Department of Mechanical Engineering
McGill University
Montreal 12, Quebec, Canada

Dr. S. S. Stahara
Nielsen Engineering & Research, Inc.
510Clyde Avenue
Mountain View, CA 94043

Engineering Societies Library
345 East 47th Street
New York, NY 10017

Professor A. Jameson
New York University
Courant Institute of Mathematical
Sciences
251 Mercer Street
New York, NY 10012

Professor G. Miller
Department of Applied Science
New York University
26-36 Stuyvesant Street
New York, NY 10003

Office of Naval Research
New York Area Office
715 Broadway - 5th Floor
New York, NY 10003

Dr. A. Vaglio-Laurin
Department of Applied Science
26-36 Stuyvesant Street
New York University
New York, NY 10003

Professor H. E. Rauch
Ph.D. Program in Mathematics
The Graduate School and University
Center of the City University of
New York
33 West 42nd Street
New York, NY 10036

Librarian, Aeronautical Library
National Research Council
Montreal Road
Ottawa 7, Canada

Lockheed Missiles and Space Company
Technical Information Center
3251 Hanover Street
Palo Alto, CA 94304

Commanding Officer
Office of Naval Research Branch Office
1030 East Green Street
Pasadena, CA 91106

California Institute of Technology
Engineering Division
Pasadena, CA 91109

Library
Jet Propulsion Laboratory
4800 Oak Grove Drive
Pasadena, CA 91103

Professor H. Liepmann
Department of Aeronautics
California Institute of Technology
Pasadena, CA 91109

Mr. L. I. Chasen, MGR-MSD Lib.
General Electric Company
Missile and Space Division
P. O. Box 8555
Philadelphia, PA 19101

Mr. P. Dodge
Airesearch Manufacturing Company
of Arizona
Division of Garrett Corporation
402 South 36th Street
Phoenix, AZ 85010

Technical Library
Naval Missile Center
Point Mugu, CA 93042

Professor S. Bogdonoff
Gas Dynamics Laboratory
Department of Aerospace and
Mechanical Sciences
Princeton University
Princeton, NJ 08540

Professor S. I. Cheng
Department of Aerospace and
Mechanical Sciences
Princeton University
Princeton, NJ 08540

Dr. J. E. Yates
Aeronautical Research Associates
of Princeton, Inc.
50 Washington Road
Princeton, NJ 08540

Professor L. Sirovich
Division of Applied Mathematics
Brown University
Providence, RI 02912

Dr. P. K. Dai (RI/2178)
TRW Systems Group, Inc.
One Space Park
Redondo Beach, CA 90278

Redstone Scientific Information Center
Chief, Document Section
Army Missile Command
Redstone Arsenal, AL 35809

U.S. Army Research Office
P. O. Box 12211
Research Triangle, NC 27709

Editor, Applied Mechanics Review
Southwest Research Institute
8500 Culebra Road
San Antonio, TX 78228

Library and Information Services
General Dynamics-CONVAIR
P. O. Box 1128
San Diego, CA 92112

Dr. R. Magnus
General Dynamics-CONVAIR
Kearny Mesa Plant
P. O. Box 80847
San Diego, CA 92138

Mr. T. Brundage
Defense Advanced Research Projects
Agency
Research and Development Field Unit
APO 146, Box 271
San Francisco, CA 96246

Office of Naval Research
San Francisco Area Office
One Hallidie Plaza, Suite 601
San Francisco, CA 94102

Library
The RAND Corporation
1700 Main Street
Santa Monica, CA 90401

Dr. P. E. Rubbert
Boeing Aerospace Company
Boeing Military Airplane Development
Organization
P. O. Box 3707
Seattle, WA 98124

Dr. H. Yoshihara
Boeing Aerospace Company
P. O. Box3999
Mail Stop 41-18
Seattle, WA 98124

Mr. R. Feldhuhn
Naval Surface Weapons Center
White Oak Laboratory
Silver Spring, MD 20910

Librarian
Naval Surface Weapons Center
White Oak Laboratory
Silver Spring, MD 20910

Dr. J. M. Solomon
Naval Surface Weapons Center
White Oak Laboratory
Silver Spring, MD 20910

Professor J. H. Ferziger
Department of Mechanical Engineering
Stanford University
Stanford, CA 94305

Professor K. Karamcheti
Department of Aeronautics and
Astronautics
Stanford University
Stanford, CA 94305

Professor M. van Dyke
Department of Aeronautics and
Astronautics
Stanford University
Stanford, CA 94305

Professor O. Bunemann
Institute for Plasma Research
Stanford University
Stanford, CA 94305

Engineering Library
McDonnell Douglas Corporation
Department 218, Building 101
P. O. Box 516
St. Louis, MO 63166

Dr. R. J. Hakkinen
McDonnell Douglas Corporation
Department 222
P. O. Box 516
St. Louis, MO 63166

Dr. R. P. Heinisch
Honeywell, Inc.
Systems and Research Division -
Aerospace Defense Group
2345 Walnut Street
St. Paul, MN 55113

Dr. N. Malmuth
Rockwell International Science Center
1049 Camino Dos Rios
P. O. Box 1085
Thousand Oaks, CA 91360

Library
Institute of Aerospace Studies
University of Toronto
Toronto 5, Canada

Professor W. R. Sears
Aerospace and Mechanical Engineering
University of Arizona
Tucson, AZ 85721

Professor A. R. Seebass
Department of Aerospace and Mechanical
Engineering
University of Arizona
Tucson, AZ 85721

Dr. K. T. Yen
Code 3015
Naval Air Development Center
Warminster, PA 18974

Air Force Office of Scientific Research
(SREM)
Building 1410, Bolling AFB
Washington, DC 20332

Chief of Research and Development
Office of Chief of Staff
Department of the Army
Washington, DC 20310

Library of Congress
Science and Technology Division
Washington, DC 20540

Director of Research (Code RR)
National Aeronautics and Space
Administration
600 Independence Avenue, SW
Washington, DC 20546

Library
National Bureau of Standards
Washington, DC 20234

National Science Foundation
Engineering Division
1800 G Street, NW
Washington, DC 20550

Mr. W. Koven
AIR 03E
Naval Air Systems Command
Washington, DC 20361

Mr. R. Siewert
AIR 320D
Naval Air Systems Command
Washington, DC 20361

Technical Library Division
AIR 604
Naval Air Systems Command
Washington, DC 20361

Code 2627
Naval Research Laboratory
Washington, DC 20375

SEA 03512
Naval Sea Systems Command
Washington, DC 20362

SEA 09G3
Naval Sea Systems Command
Washington, DC 20362

Dr. A. L. Slafkosky
Scientific Advisor
Commandant of the Marine Corps
(Code AX)
Washington, DC 20380

Director
Weapons Systems Evaluation Group
Washington, DC 20305

Chief of Aerodynamics
AVCO Corporation
Missile Systems Division
201 Lowell Street
Wilmington, MA 01887

Research Library
AVCO Corporation
Missile Systems Division
201 Lowell Street
Wilmington, MA 01887

AFAPL (APRC)
AB
Wright Patterson, AFB, OH 45433

Dr. Donald J. Harney
AFFDL/FX
Wright Patterson AFB, OH 45433